

We are IntechOpen, the world's leading publisher of Open Access books Built by scientists, for scientists

6,900

Open access books available

186,000

International authors and editors

200M

Downloads

Our authors are among the

154

Countries delivered to

TOP 1%

most cited scientists

12.2%

Contributors from top 500 universities



WEB OF SCIENCE™

Selection of our books indexed in the Book Citation Index
in Web of Science™ Core Collection (BKCI)

Interested in publishing with us?
Contact book.department@intechopen.com

Numbers displayed above are based on latest data collected.
For more information visit www.intechopen.com



Orbital Control on Carbonate-Lignite Cycles in the Ptolemais Basin, Northern Greece – An Integrated Stratigraphic Approach

M.E. Weber¹, N. Tougiannidis¹, W. Ricken¹,
C. Rolf², I. Oikonomopoulos³ and P. Antoniadis³

¹University of Cologne

²Leibniz Institute for Applied Geosciences

³National Technical University of Athens

^{1,2}Germany

³Greece

1. Introduction

Establishing the time frame is crucial for most geoscientific investigation. Without proper time control, past geologic processes cannot be inferred appropriately, nor can their dynamics be understood adequately. Rhythmic changes in sedimentary cycles hold the key to establishing precise and high-resolution chronologies. The concept goes back to theoretical considerations first published by Milankovitch (1941). His calculations showed that changes in earth's orbital geometry lead to changes in the seasonal and latitudinal distribution of incoming solar radiation (insolation). Three main periods are responsible for these insolation changes, eccentricity (the shape of the orbit around the sun; with periods of 413 kyr, 123 kyr, and 95 kyr), obliquity (the tilt of the axis; changing at a period of 41 kyr), and precession (the wobbling spin of the axis with periods of 19 kyr and 23 kyr). He argued that these changes caused the waning and waxing of polar ice sheets. More than three decades later, Hays et al. (1976) and Imbrie et al. (1984) provided proof the cyclic changes of the earth energy budget were large enough to be preserved in marine sediment. Theoretical calculation of Berger (1976) and Berger and Loutre (1991) supported the Milankovitch theory and provided templates for orbital variability for the last couple of million years. Henceforth, cyclic changes in sediment strata were used to develop detailed orbital chronologies by assigning sedimentary cycles to orbital cycles.

Magnetic polarity stratigraphy is a necessary and independent tool to retrieve chronometric information for time series covering millions of years. It is based on polarity changes of the Earth's magnetic field measured over the oceans and correlated to dated magnetic polarity reversals found on land (Heirtzler et al., 1968). The presently accepted geomagnetic polarity timescale (GPTS) is the one from Cande and Kent (1995). Langereis & Hilgen (1991) and Hilgen et al. (1995) provided the first astronomical age scale for the Pliocene Capo Rosello sections in Sicily based on the GPTS. Their work was further substantiated by Krijgsman et al. (1995). For the Late Neogene, the GPTS is rather precise thanks to accurate radiometric dating methods such as ⁴⁰Ar/³⁹Ar (Kuiper et al., 2004).

A first, low-resolution, orbital-based chronology for the continental Ptolemais Basin (Fig. 1) was introduced by Steenbrink et al. (1999) and van Vugt et al. (2001; 1998). They ascribed cyclic changes of carbonates and lignites to orbital variability: maxima in lake carbonate correlate to maxima in insolation (and minima in precession). Accordingly, lignite maxima correlate to minima in insolation (i.e., beige layers in Capo Rosello). Also, they carried out extensive radiometric dating using $^{40}\text{Ar}/^{39}\text{Ar}$ (e. g., Kuiper, 2003) and delivered a high-quality composite stratigraphy for the Ptolemais Basin (Steenbrink et al., 2006). Also, Weber et al. (2010) published an orbital-based chronology for the two Upper Miocene lignite quarries Vegora and Lava. Therefore, there is robust and reliable stratigraphic information available we could base our investigations on.

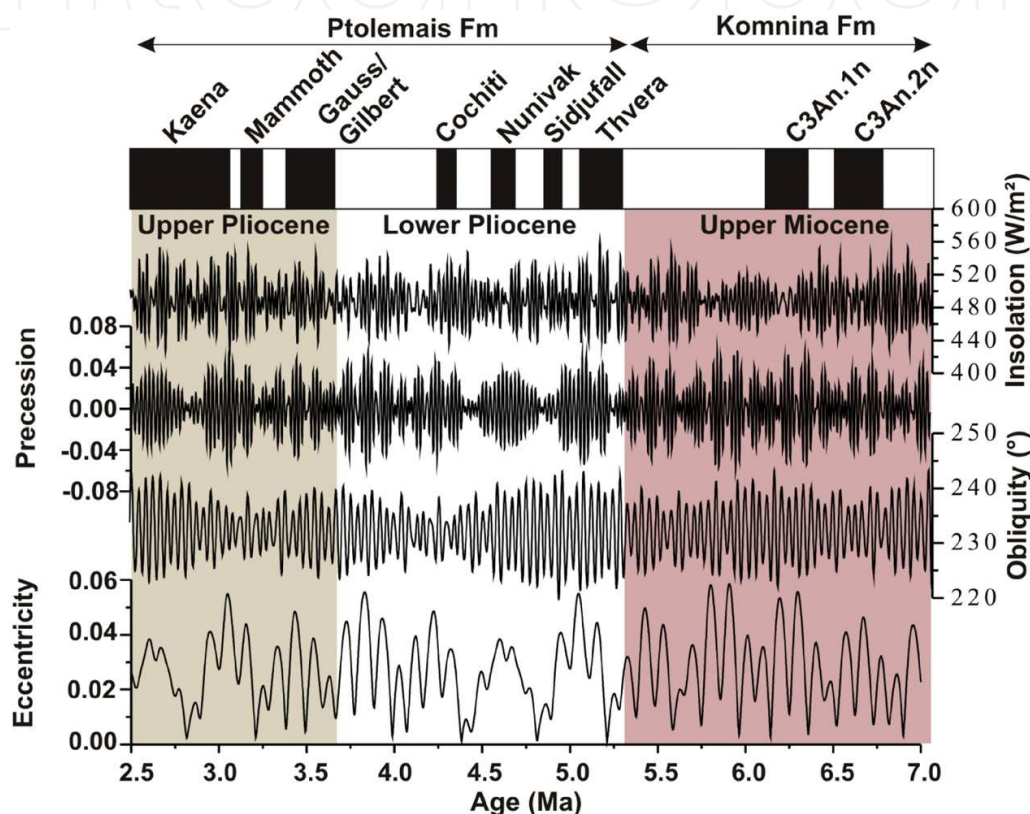


Fig. 1. Stratigraphic positions for the Ptolemais and Komnina Formations, northern Greece (e. g., Steenbrink, 2001), and magnetic chrons (black and white pattern; ages according to Cande & Kent, 1995) for the Upper Miocene to the Upper Pliocene. Curves display orbital variations of eccentricity, obliquity, precession, and the incoming solar radiation (insolation; all parameters calculated according to Laskar et al., 2004).

So far, most stratigraphic information comes from rather short outcrops in quarries and interpretations mainly rely on composite records. We investigated, for the first time, a long and continuous section (drilling KAP-107), covering the entire Lower Pliocene in a single borehole. Our goal therefore was to collect multiple high-resolution and continuous paleoclimate proxy data to establish both the orbital chronology and reconstruct paleoclimate variability during the Lower Pliocene, a time of extensive lignite formation in the Ptolemais Basin. The coal formation is sandwiched between two important events: the Upper Miocene Messinian Salinity Crisis, a time of severe constriction in the Mediterranean realm with multiple evaporation events from 5.96 – 5.33 Ma (Krijgsman et al., 1999), and the Upper Pliocene onset of northern hemisphere glaciation.

2. The Ptolemais basin

The Ptolemais Basin (Fig. 2) is a SSE – NNW elongated intramontane Basin. Together with two flanking mountain ranges, the Askion to the west and the Vermion to the east, it belongs to the Pelagonian Zone (Bornovas & Rondogianni-Tsiambaou, 1983). The Ptolemais Basin formed during the Late Neogene in northwestern Greece (Pavlidis & Mountrakis, 1987) and contains lacustrine deposits of Upper Miocene to Quaternary age (up to 800 m thick; Anastopoulos & Koukouzas, 1972) with an extended Lower Pliocene alternation of lignites, clays, and marls. The depositional history reflects interaction of orbital forcing and tectonic movement (Steenbrink et al., 2006; Tougiannidis, 2009). Through continued Pleistocene extension, the Basin is further subdivided into the basins of Florina-Vevi, Amynteon-Vegora, Ptolemais, and Kozani-Servia (Antoniadis et al., 1994), where a number open pit mines and active coal mining fields are located (Tougiannidis, 2009). The deposits are highly fragmented due to fault tectonics.

Borehole KAP-107 was drilled for exploration purposes in 2006 by the Public Power Cooperation (PPC) in the Amynteon lignite field, 12 km northwest of the city of Ptolemaida (at 40°37'3" N and 21°37'20" E). It is 233 m long and has variable borehole diameters of 18 – 8 cm (top to bottom). We investigated the lowermost part between 72 m and 230 m in detail.

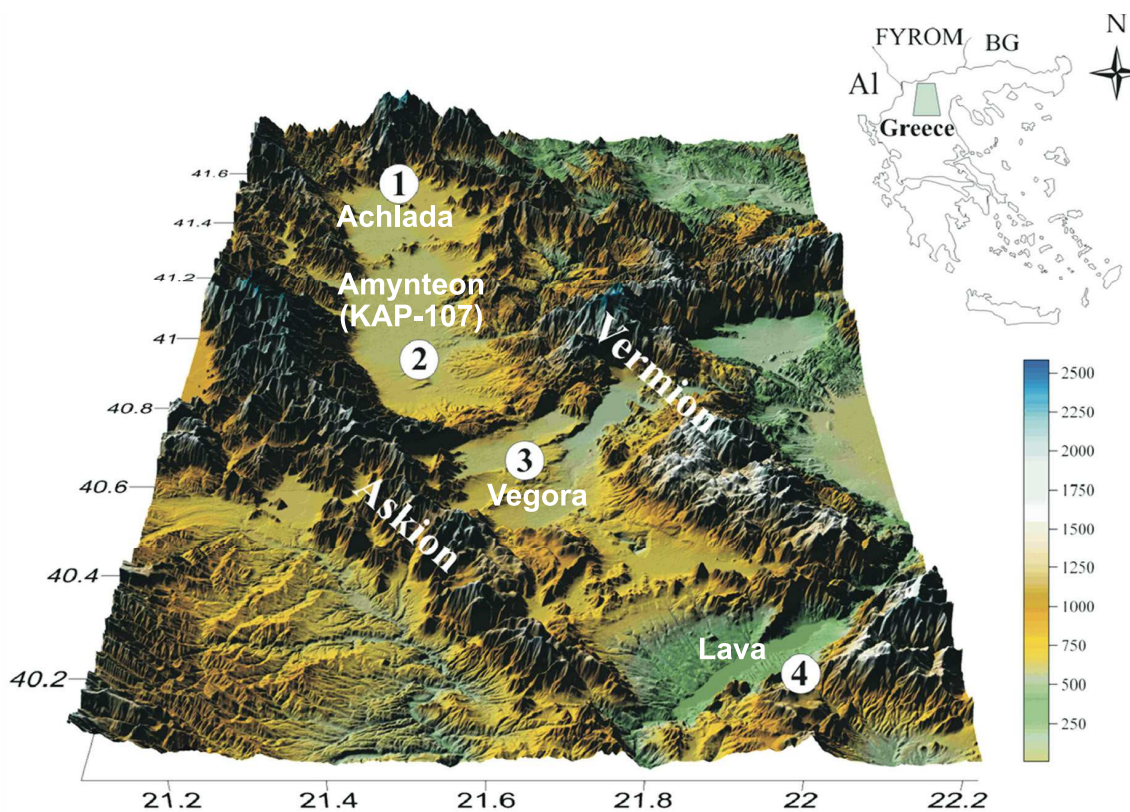


Fig. 2. 3-D location map of the Ptolemais Basin in northern Greece. The NNW – SSE elongated basin is flanked by the mountain ranges Askion in the west and Vermion in the east. Numbers indicate the four research sections referred to in this study: 1 – Achlada, 2 – Amynteon with borehole KAP-107, 3 – Vegora, and 4 – Lava. Data from sections Vegora and Lava are published in Weber et al. (2010). For digital elevation data see <http://srtm.csi.cgiar.org>.

3. Analytical methods

The methods of this study rely primarily on high-resolution non-destructive color measurements. As a fundamental sediment property color is often used for lithologic differentiation and to determine sedimentological structures, facies etc. We measured a total of approximately 16,500 samples non-destructively for color variability using a Minolta Chromatometer CM–2002. This hand-held system is easy to use in the field. There is hardly any maintenance and measurements can be conducted quickly and cost effective. Measurements were made on clean and fresh (scraped with a spatula) surfaces at 1-cm resolution, using the CIELAB color model “L*-a*-b*”. The system provides three color values for each measurement (details see Weber, 1998): the L* axis (the black-white color component), also known as lightness or grey value; the a*axis (the green/red component); and the b*axis (the yellow/blue component). Together, the three parameters describe coordinates in a spherical system (16 million possible variations). Measurements of C* describe the chroma (colorfulness). The difference between two successive color coordinates (ΔE^*_{ab}) was calculated as $\Delta E^*_{ab} = \sqrt{(\Delta L^*)^2 + (\Delta a^*)^2 + (\Delta b^*)^2}$. Since ΔE^*_{ab} contains the variability of all three color components, we refer to it as the whole color difference.

Paleomagnetic measurements were made on discrete samples in the lab. We determined natural remanent magnetization (NRM) and alternating-field demagnetization (AF) to generate the characteristic remanent magnetization (ChRM) (Tougiannidis, 2009). A total of 200 completely oriented diamagnetic sample cubes of 12 cm³ were retrieved at 80-cm intervals on average. NRM was measured in x and y direction using a cryogenic spin magnetometer (2G Enterprises). We applied AF before inclination and declination was measured and used orthogonal projections (Zijderveld, 1967) to correct the values for noise before using them for magnetostratigraphy.

We used the Analyseries software (Paillard, 1996) to perform astronomical tuning experiments and to construct age-depth models. Orbital parameters for the time frame 6 – 3 Ma were calculated in 1-kyr increments (see Fig. 1) for eccentricity, obliquity, precession, using the solutions provided by Laskar et al. (2004). Orbital insolation was calculated for the month of June at 40°N to reflect the approximate energy budget of the site.

We used ESALAB (Weber et al., 2010) to study of the resulting time series for frequency pattern and to compare them to orbital time series. ESALAB conducts both bulk and evolutionary spectral analysis (ESA). The program relies on the Lomb (1976) and Scargle (1982, 1989) algorithms, and provides an estimate of the spectrum by fitting harmonic sine and cosine components to the data set. This has two decisive advantages: the input data can be unequally spaced and the resulting spectra are rather robust and of high resolution. While performing the Fourier transformation, both window length and step size are freely adjustable. Also, the window type is selectable among Hanning, Hanning, Blackman, sin², and boxcar. The output consists of graphic files for bulk and ESA spectra and tabulated data. The sample increment of 1 cm puts the Nyquist frequency (the highest frequency detectable) at 0.5 cm⁻¹, i.e., the spatial resolution for bulk and ESA is 2 cm.

4. Ground-truth stratigraphy

Ground-truth stratigraphy for borehole KAP-107 relies on paleomagnetic data (see Table 1). The site shows a flickering pattern of revers and normal polarity (Fig. 3). Inclination and

declination values vary -4 – -67° and 359 – 6° for revers polarity, respectively, and 1 – 84° and 358° for normal polarity. Pronounced reversals occur at 141.1 m, 147.55 m, 165.14 m, 167.55 m, 172.88 m, 178.92 m, 191.24 m, 203.35 m, 215.1 m, and 220.93 m. Although the sample resolution of 80 cm (see above) is relatively low, the combination of inclination and declination changes provides a trustworthy reversal pattern that can be applied rather confidently. With the exception of 165.14 – 167.55 m, all remaining sections of normal polarity can confidently be assigned to chrons Gauss/Gilbert, Cochiti, Nunivak, Sidjufall, and Thvera (Fig. 3).

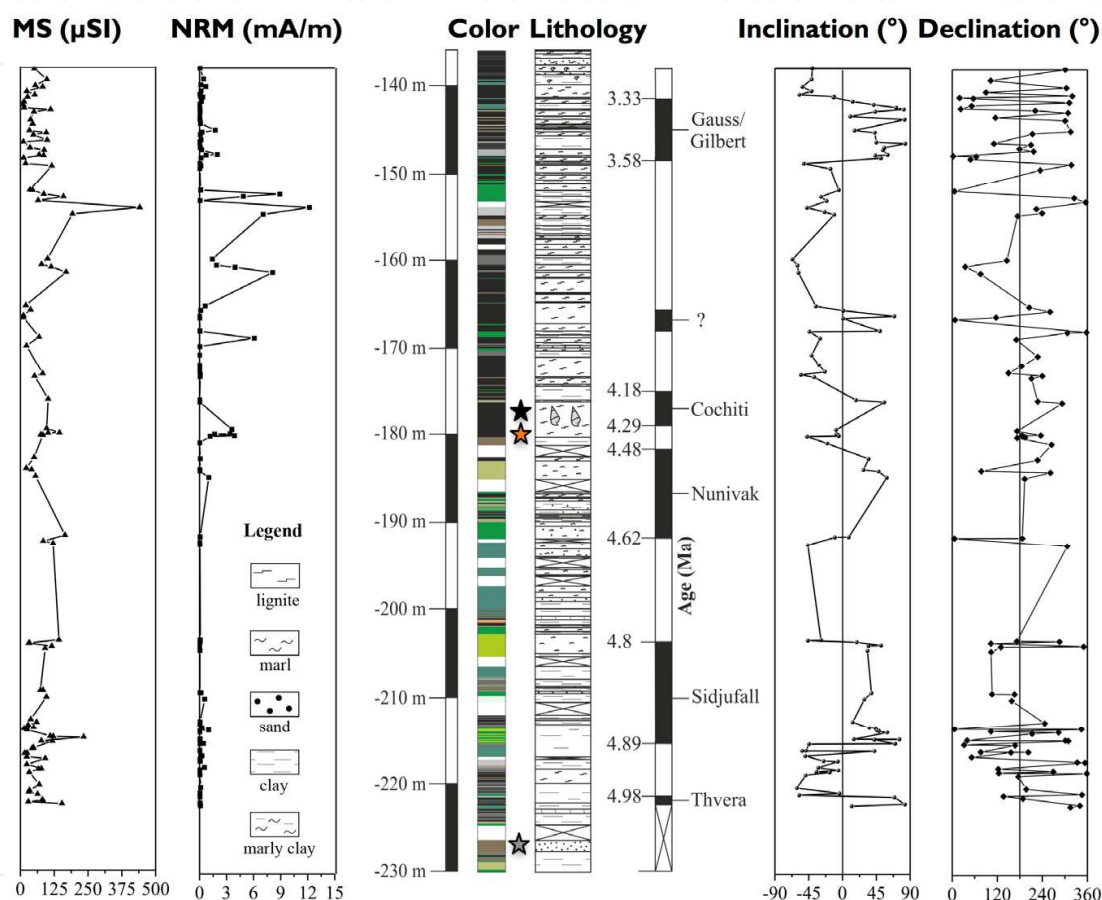


Fig. 3. Paleomagnetic ground-truth stratigraphy for borehole KAP-107. From left to right are magnetic susceptibility (MS), natural remanent magnetization (NRM), visual color, lithology, magnetic chron assignment, inclination, and declination. Age assignments are according to the age scale of Krijgsman et al. (1999). Black star represents the Neritina marker bed. This shell horizon belongs to the Theodoxus Member and has an age of roughly 4.4 Ma (orange star) according to $^{40}\text{Ar}/^{39}\text{Ar}$ dating of Steenbrink (2001). Grey star shows a glauconite horizon that has an approximate age of 5 Ma. Details see text.

Our age assignment is corroborated by additional sedimentologic and biostratigraphic evidence. Unpublished records of the Federal Institute for Geosciences and Natural Resources (BGR, Hannover, Germany) from 1960 – 1970 mention a glauconite horizon just above the onset of sedimentation in the entire Ptolemais Basin, after the termination of the Messinian Salinity Crisis. We detected this layer at borehole KAP-107 in 228 m (Fig. 3), where the magnetic reversal pattern indicates the top of the Thvera chron (dated to

4.98 Ma). Also, we found the Neritina marker (*Theodoxus Macedonicus* WENZ, 1943) bed in roughly 174 - 178 m. This shell horizon belongs to the Theodoxus member and has an age of roughly 4.4 Ma (Steenbrink, 2001), which is in good agreement to 4.48 - 4.29 Ma deduced from our magnetic dating for this depth section.

Borehole KAP-107 was drilled to the depth where lignite deposition commenced in the Ptolemais Basin. According to our magnetic dating, the lowermost part of the core (underneath 222 m) belongs to the Thvera subchron and is hence somewhat older than 4.98 Ma. These stratigraphic results are inline with Steenbrink et al. (2006), who dated the onset of extensive lignite sedimentation approximately to the base of the Thvera subchron at 5.23 Ma. Hence there appears to be a lag time of approximately 100 kyr to the end of the Messinian Salinity Crisis that dates to 5.33 Ma (Krijgsman et al., 1999), and is marked by rapid re-flooding of the entire Mediterranean Basin (Garcia-Castellanos et al., 2009).

In summary, borehole KAP-107 represents continuous sedimentation during the entire Lower Pliocene. It covers a duration of 2 myr from 5.1 - 3.1 Ma. The resulting low-resolution age model comprises nine confident age control points (Table 1) from reversal dating and two additional evidences that support the stratigraphic assignment. Sedimentation rates are 14 - 2 cm/kyr, with an average rate of 6 cm/kyr, and a decreasing tendency towards the top of the borehole.

5. Cyclic variability of high-resolution color data

We measured a total of five sediment-optical data sets (L^* , a^* , b^* , C , ΔE^*ab). Most of them characterize facies changes and show striking cyclic variability (Figs. 4 and 5). The advantage of using a number of different sediment proxy records is that various aspects of changing sediment composition and supply and the relation to climate forcing can be addressed simultaneously.

Specifically sediment lightness shows a striking pattern of highs and lows with brighter (marl-rich) and darker (clay-rich or lignite-rich) intervals, and the coal seams as the darkest parts. Therefore, L^* is generally a good indicator for either calcium carbonate (high values) contents (see also Weber, 1998) or organic carbon and/or lignite (low values). The similarity to the whole color difference ΔE^*ab reveals that, for the most part, changes in L^* dominate color variability. Initial spectral analysis of L^* in the depth domain revealed sedimentary cycles ranging from 0.4 to 2.4 m, with a dominance centered around 1 - 1.4 m, and a tendency to become shorter with shallower core depths.

Color values a^* , b^* , and C^* show lower-amplitude cycles and a clear increase in values to the top (Fig. 4). Specifically the sections shallower than approximately 92 m indicate an elevated plateau. Higher b^* values reflect elevated contents of yellowish iron oxides (e. g., above 95 m core depth), most likely caused by the presence of hematite and goethite (see Weber et al., 2010). Low b^* values refer to bluish components, abundant in bitumen or coal (mostly the sections underneath 135 m), or provided by sulfides.

The red-green variation (color value a^*) provides an indication for the redox conditions, although the signal might be influenced by diagenetic overprint. Oxidic conditions are indicated for core sections shallower than 95 m; the depths underneath show low-amplitude variations between slightly reduced and slightly oxidic. The co-variability of color component C^* throughout the record reveals that a^* values primarily determine the chroma (Fig. 4).

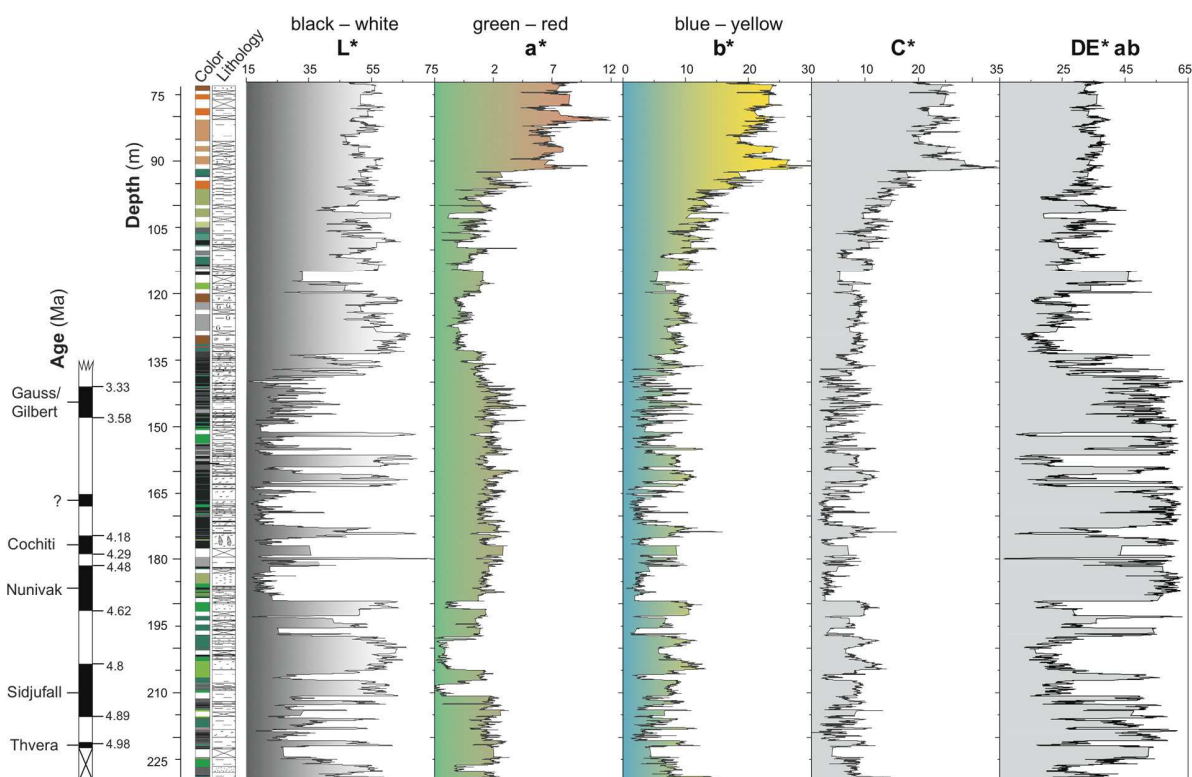


Fig. 4. Non-destructive color data from borehole KAP-107. From left to right are paleomagnetic reversals, visual color, lithology, sediment lightness (L^*), red-green component (a^*), yellow-blue component (b^*), chroma (C^*), and whole color difference (ΔE^*ab). Note that, only for graphical considerations, all high-resolution data have been smoothed using an 11-point Gaussian filter. Note further that L^* provides an estimate for either organic carbon or carbonate; a^* indicates the redox state, and b^* yields information about the iron oxide content.

6. Astronomical tuning

The process by which past variations in earth's orbit are correlated to the cyclic variability of sediment parameters is called astronomical or orbital tuning. In the Ptolemais Basin, we tuned the cyclic lignite marl alternations to orbital time series, using the algorithms of Laskar et al. (2004), and relying on the magnetic polarity time scale of Krijgsman et al. (1999) as ground-truth stratigraphy (Fig. 5).

Accordingly, we first generated a low-resolution age model for borehole KAP-107 by using the nine magnetostratigraphic fix points of Table 1 (see blue dots in Fig. 5) and converting core depths into ages linearly between tie points. As a tuning target, we used the insolation curve for the month of June at $40^\circ N$ according to Laskar et al. (2004). Since magnetostratigraphy was only available for the lignite-bearing sections (135 – 223 m), we conducted the experiments only for the time interval 5.3 – 3.1 Ma.

Given the magnetostratigraphic boundaries and sedimentary cycles of 0.4 to 2.4 m with a dominance of 1 – 1.4 m (see above), calculated sedimentation rates vary from 2 to 12 cm/kyr with an average of 6 cm/kyr. This translates into a cycle length of roughly 1.2 m per precession (insolation) cycle, and 5 – 6 m per eccentricity cycle. Exactly these two frequencies are dominant in the L^* and ΔE^*ab records as lower and higher amplitude cycles, respectively (Fig. 5).

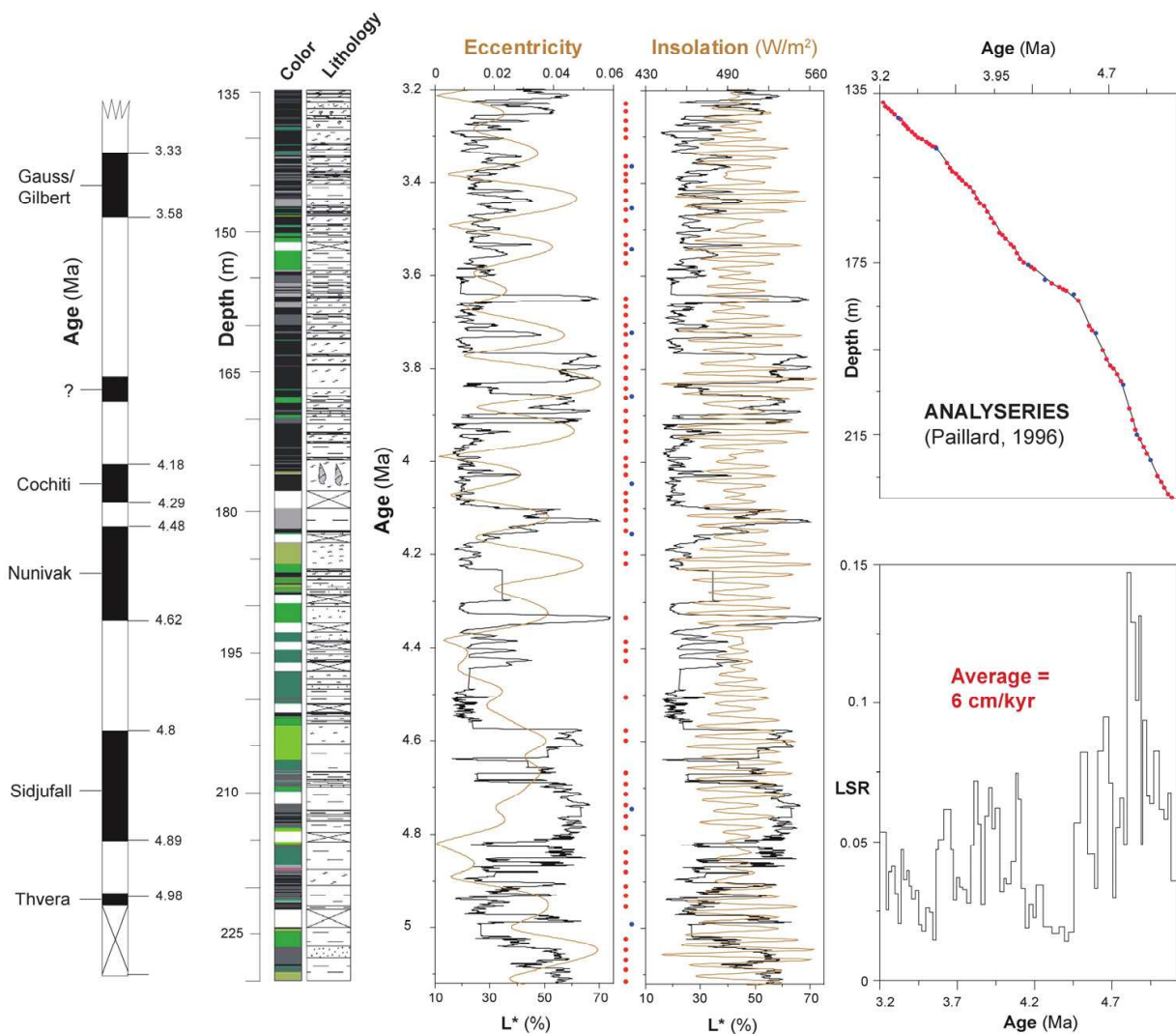


Fig. 5. Orbital tuning of borehole KAP-107. Sediment lightness (L^*) of borehole KAP-107 tuned versus orbital insolation. From left to right are magnetic reversal pattern, visual color, lithology, sediment lightness L^* versus orbital eccentricity, and L^* versus orbital insolation at 40°N for the month of June (data from Laskar et al., 2004). Histograms to the right give age-depth relationship (top) and linear sedimentation rates (LSR) between tuned tie points (bottom). Note that carbonate maxima were tuned to insolation maxima (red dots) to concur with the procedure introduced by Steenbrink et al. (2006; 2000). Blue dots give ages of ground-truth stratigraphy.

Steenbrink et al. (2000) pointed out that dark-colored marls correspond to relatively dry periods, whereas light-colored marls represent more humid periods (lake-level highstands). Since humid climate in the Mediterranean occurred during insolation maxima (e. g., Emeis et al., 2000), we used the insolation curve for the month of June at 40°N according to Laskar et al. (2004) and tuned individual carbonate maxima between the magnetostratigraphic tie points to insolation maxima. Thereby, we increased the resolution of the age model to an additional 70 age control points without violating the ground-truth boundaries provided by Table 1. Weber et al. (2010) followed the strategy of Steenbrink et al. (2006; 2000) and tuned insolation minima to dark intervals. However, the KAP-107 record contains broad lows and

| Depth (m) | Age (Ma) | Remark | Sed. rate (cm/kyr) | Depth (m) | Age (Ma) | Remark | Sed. rate (cm/kyr) |
|-----------|----------|-------------|--------------------|-----------|----------|---------------|--------------------|
| 137.39 | 3.231 | ITP | 5.3 | 170.62 | 4.068 | ITP | 4.3 |
| 138.37 | 3.249 | ITP | 2.5 | 171.39 | 4.086 | ITP | 7.5 |
| 138.86 | 3.269 | ITP | 3.9 | 172.78 | 4.105 | ITP | 6.5 |
| 139.57 | 3.287 | ITP | 4.1 | 174.23 | 4.127 | ITP | 3.3 |
| 140.31 | 3.304 | Ga/Gilb (t) | 3.1 | 174.96 | 4.149 | ITP | 1.9 |
| 141.10 | 3.330 | ITP | 2.1 | 175.54 | 4.180 | Cochiti (t) | 2.7 |
| 141.42 | 3.345 | ITP | 4.7 | 176.05 | 4.198 | ITP | 2.2 |
| 142.44 | 3.367 | ITP | 3.6 | 176.54 | 4.221 | ITP | 3.4 |
| 143.04 | 3.384 | ITP | 4.0 | 178.92 | 4.290 | Cochiti (o) | 1.9 |
| 143.61 | 3.398 | ITP | 3.4 | 179.80 | 4.335 | Neritina (t) | 1.7 |
| 144.31 | 3.418 | ITP | 2.9 | 180.65 | 4.385 | ITP | 1.9 |
| 144.93 | 3.439 | ITP | 3.2 | 181.06 | 4.406 | ITP | 1.4 |
| 145.60 | 3.460 | ITP | 2.0 | 181.37 | 4.428 | ITP | 1.7 |
| 146.05 | 3.483 | ITP | 1.8 | 182.27 | 4.480 | Nunivak (t) | 5.7 |
| 146.60 | 3.514 | ITP | 2.6 | 183.76 | 4.506 | Neritina (o) | 8.2 |
| 147.12 | 3.534 | ITP | 2.5 | 189.55 | 4.577 | ITP | 4.5 |
| 147.64 | 3.555 | ITP | 1.4 | 190.56 | 4.599 | ITP | 3.3 |
| 147.91 | 3.574 | ITP | 4.7 | 191.26 | 4.620 | Nunivak (o) | 8.2 |
| 148.18 | 3.580 | G/Gilb(o) | 5.1 | 195.27 | 4.669 | ITP | 9.5 |
| 151.71 | 3.649 | ITP | 6.1 | 197.50 | 4.692 | ITP | 7.1 |
| 152.80 | 3.667 | ITP | 4.7 | 199.06 | 4.714 | ITP | 3.0 |
| 153.65 | 3.685 | ITP | 2.9 | 199.76 | 4.738 | ITP | 5.5 |
| 154.27 | 3.707 | ITP | 3.7 | 201.07 | 4.761 | ITP | 6.5 |
| 155.00 | 3.726 | ITP | 3.4 | 202.60 | 4.785 | ITP | 4.9 |
| 155.75 | 3.748 | ITP | 3.3 | 203.35 | 4.800 | Sidjufall (t) | 14.7 |
| 156.60 | 3.774 | ITP | 2.8 | 209.03 | 4.839 | ITP | 12.9 |
| 157.27 | 3.799 | ITP | 4.9 | 211.83 | 4.860 | ITP | 10.1 |
| 158.35 | 3.821 | ITP | 7.2 | 213.92 | 4.881 | ITP | 13.1 |
| 159.88 | 3.842 | ITP | 5.6 | 215.10 | 4.890 | Sidjufall (o) | 4.9 |
| 161.02 | 3.862 | ITP | 2.7 | 216.14 | 4.911 | ITP | 9.4 |
| 161.84 | 3.892 | ITP | 5.9 | 218.07 | 4.932 | ITP | 6.6 |
| 163.12 | 3.914 | ITP | 6.9 | 219.63 | 4.955 | ITP | 6.3 |
| 164.62 | 3.936 | ITP | 5.5 | 221.20 | 4.980 | Thvera (t) | 8.3 |
| 165.74 | 3.956 | ITP | 6.2 | 224.93 | 5.025 | Glauconite | 6.1 |
| 168.01 | 3.993 | ITP | 3.2 | 226.31 | 5.048 | ITP | 5.8 |
| 168.56 | 4.010 | ITP | 3.7 | 227.60 | 5.070 | ITP | 6.7 |
| 169.27 | 4.029 | ITP | 3.5 | 229.01 | 5.091 | ITP | 3.6 |
| | | | | 229.94 | 5.117 | ITP | 3.6 |

Table 1. Age model for borehole KAP-107. Integer numbers refer to ground-truth stratigraphy from paleomagnetic reversal dating (age scale according to Cande & Kent, 1995; Krijgsman et al., 1999), from $^{40}\text{Ar}/^{39}\text{Ar}$ dating of the Neritina bed and a glauconite horizon (van Vugt et al., 1998). Remaining age control points result from tuning color component L* to orbital insolation (data from Laskar et al., 2004). Sedimentation rates are given in cm/kyr. Ga/Gilb refers to magnetic chrons Gauss/Gilbert. ITP stands for insolation tuning point.

sharp highs in the L^* record, so the tuning the other half of the insolation cycle, i. e., insolation maxima to bright intervals, seemed more appropriate and accurate. In any way, we obtained about the same resolution in the tuned age models as in previous studies and the age models are congruent. To establish the correlation between climate proxy variability and orbital parameter in the time domain was rather easy and straight forward; hence, the resulting stratigraphic model appears robust and reliable with tuned age control points at (ideally) every insolation maximum (every 20 kyr; see Table 1). The only uncertainties resulted from some missing core sections, where we had to interpolate the ages (see Fig. 5).

The resulting high-resolution age model comprises an additional 70 age control points and indicates a preservation period for KAP-107 of almost precisely 2 myr (5.12 – 3.09 Ma). Sedimentation rates were quite variable over this rather long period. Specifically the lower part of the Ptolemais Formation (for formation names see Fig. 7) shows elevated and variable values during the Kyrio member, followed by very low values during the Theodoxus member, intermediate values during the Notio member, and low to intermediate values during the Anargyri member (Fig. 5). Compared to Upper Miocene sections Lava and Vegora, borehole KAP-107 indicates that the Amynteon Basin received only 20 – 30 % of the sediment material during the Lower Pliocene.

7. Spectral analysis

Spectral analysis in the depth domain is ambiguous when changes in sedimentation rate occur, because the amplitude of the response will be reduced or even be absorbed. Borehole KAP-107 exhibits quite some variability in sedimentation rates; hence we transformed the depth series first into the time domain using the ground-truth age control points (see blue dots in Fig. 5). Only then, we conducted bulk and evolutionary spectral analyses to decide about the following tuning procedure.

In the spectra we mainly found eccentricity and precession cycles (Fig. 6). This is not surprising because precession contributes a substantial part to the insolation forcing in low-to-mid latitudes. Orbital eccentricity modulates the amplitude of the precession cycle (Imbrie et al., 1993) and is therefore also important for the Ptolemais Basin (Steenbrink et al., 2006), specifically in the lower sedimentation-rate sites (Tougiannidis, 2009). Steenbrink et al. (2006) also found a robust obliquity signal in some parts of section Lava. However, obliquity has virtually no impact for borehole KAP-107, which is also not surprising since this frequency is related to the changing tilt of the earth and therefore mainly observable at higher latitudes (e. g., Weber et al., 2001), where it is mostly associated with the presence of larger ice sheets (e. g., Ruddiman, 2004).

Given the average sedimentation rates of 6 cm/kyr and the sampling increment of 1 cm, the average sample resolution is roughly 170 years. This resolution is enough to also be able to detect suborbital (millennial-to-centennial-scale) signals. However, the precession signal is so dominant that higher frequencies are not apparent in the time series, although rhythmic bedding in the cm to dm band can be observed in the outcrop. Either this type of bedding is autocyclic, i. e., it results from basin-internal processes that are not linked to orbital or solar forcing, or, more likely, post-sedimentary compaction operates different on the various facies types, thereby altering the depth-age relationship that has originally been established. Alternatively, different facies types may have been deposited at different rates. In any case, the age control points are only precession-controlled and hence cannot resolve these high-frequencies variations.

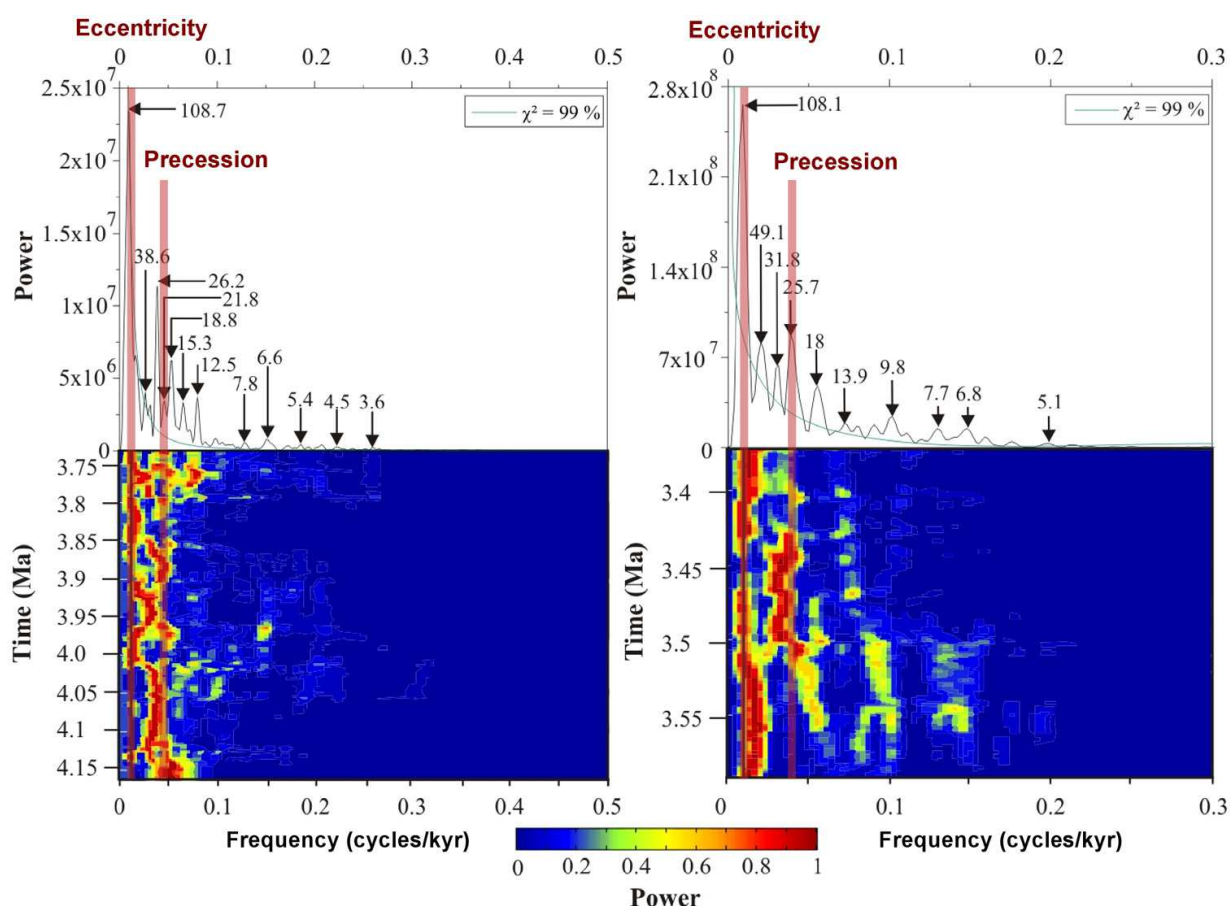


Fig. 6. Spectral analysis of color component L^* for borehole KAP-107 for two time slices 4.2 – 3.7 Ma (left) and 3.6 – 3.35 Ma (right). Bulk spectra (top) were calculated using REDFIT software (Schulz & Mudelsee, 2002). Green line shows the 99 % confidence interval. Evolutionary spectral analyses (bottom) were calculated with ESALAB software (Weber et al., 2010) with a window size of 100 kyr and a shift of 5 kyr from one analysis to the next.

8. Age model discussion and chronostatigraphic correlation

Rhythmic bedding of sedimentary sequences reflects mostly the response to cyclic changes in earth's orbital geometry, namely eccentricity, obliquity, and precession. Changes in orbital parameters lead to changes in insolation with respect to season and latitude. For a given repetitive sedimentary succession we can use this relationship to establish a high-resolution and precise chronology. This requires, however, other means of stratigraphic control such as biostratigraphic markers or the orientation of magnetic grains, which are locked immediately after the time of deposition. The magnetic reversal pattern, on the other hand, can precisely be dated and yields the foundation of the geomagnetic polarity time scale (GPTS, Cande & Kent, 1995). At least for the Late Neogene, the dating accuracy for magnetic reversals is sufficient to establish orbital chronologies (e. g., Hilgen et al., 1995).

Obtaining independent stratigraphic information is crucial because there might also be autocyclic processes (see above) that create rhythmic bedding. Here, single crystal $^{40}\text{Ar}/^{39}\text{Ar}$ dating using the laser fusion technique provided an essential step forward (e. g., Kuiper et al., 2004).

Once a low-resolution age control is established, spectral analysis can reveal whether or not rhythmic bedding is related to orbital frequencies. Because this was the case, we were able to “tune” sedimentary cycles to orbital frequencies. This rather simple and straightforward approach yields a very powerful stratigraphic tool – the resulting time series provide age models of previously unmatched resolution and precision.

We also followed this strategy and dated borehole KAP-107 using magnetic polarity changes and additional stratigraphic evidence. The resulting low-resolution age model indicated spectral power on the eccentricity band and thereby showed that orbital forcing is the likely cause for rhythmic bedding. We used this information to tune the greyscale (L^*) variability to orbital insolation. As a result, we obtained a precession-controlled age model over 2 myr of deposition in the Lower Pliocene, from 5.1 to 3.1 Ma. The age model provides, ideally, one control point every 1.2 m – enough for a very detailed reconstruction of the depositional history of any given environment.

In the next step, we applied the tuning method to a number of mining fields and outcrops from the Ptolemais Basin (see Fig. 7). Our chronology, again, is tied into the chronology of the composite record that has been established by Steenbrink et al. (1999) for the Ptolemais Basin. As a result, we obtained a complete sedimentary record from the Upper Miocene section Achlada (this study) and sections Lava and Vegora (Weber et al., 2010) to the Upper Pliocene (borehole KAP-107; this study), from roughly 7 to 3 Ma at precession-scale age control, with the exception of the Messinian Salinity Crisis from 5.9 to 5.33 Ma (Krijgsman et al., 1999).

Combined biomagnetostratigraphy and orbital tuning revealed that lacustrine sections Vegora and Lava from the central and southern Ptolemais Basin represent the period 6.85 – 6.57 Ma and 6.46 – 5.98 Ma at sedimentation rates of roughly 14 and 22 cm/kyr, respectively (Weber et al., 2010). Section Achlada from the northern edge of the Ptolemais, however, contains fluvial influence and shows less-convincing paleomagnetic evidence. According to Koukouzas et al. (2010; 2009) the Achlada deposits belong to the Komnina lignite sequence, which is why we tentatively correlated them to chron C3An.1n (Fig. 7).

Times of sediment deposition and lignite formation in the Ptolemais Basin were related to large-scale and global events. The Upper Miocene represented a global cooling (Billups, 2002; Billups et al., 2008) with lacustrine and fluvial input in the Ptolemais Basin (Steenbrink et al., 2006) and occasional lignite formation. The Messinian Salinity Crisis is characterized by at least partial desiccation in the Mediterranean realm (CIESM Workshop, 2007). Reworked alluvial to fluvial deposits dominated in the Ptolemais Basin. During the Lower Pliocene greenhouse warming accompanied the emerging Isthmus of Panama and enhanced oceanic overturning circulation (Brierley et al., 2009; Ravelo et al., 2004; Ravelo et al., 2006). Borehole KAP-107 covers this time of extensive lignite formation in the Ptolemais Basin.

During the Upper Pliocene continental ice sheets built up in the Northern Hemisphere between 3.6 and 2.4 Ma (Mudelsee & Raymo, 2005). A threshold towards full glacial to interglacial conditions occurred near 2.7 Ma (e. g., Ruggieri et al., 2009; Shackleton et al., 1984). This is broadly the time when lignite formation ceased in the Ptolemais Basin and coarser-grained, more oxic sediments were again deposited.

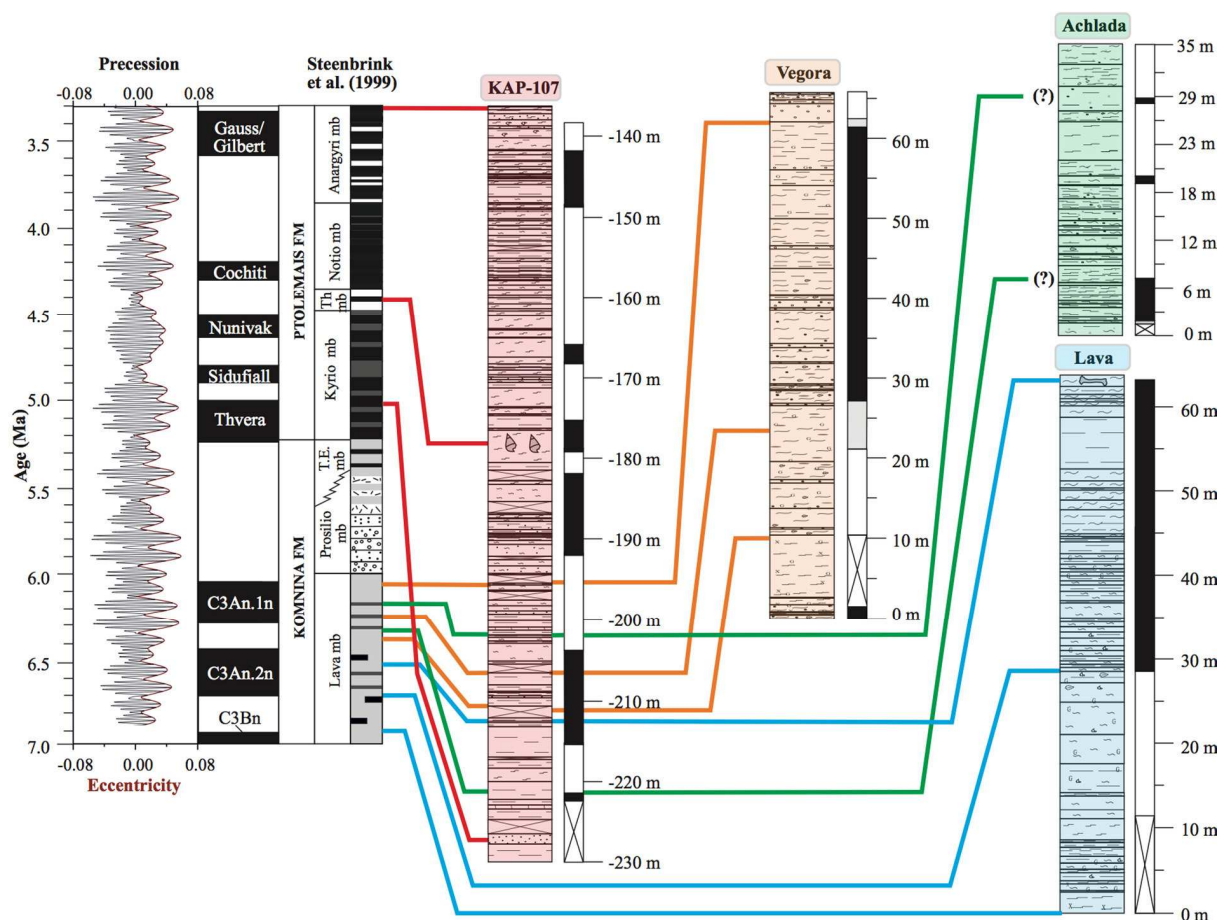


Fig. 7. Correlation of the four sites investigated in the Ptolemais Basin, spanning the time from roughly 7 Ma (chron C3Bn) to 3.3 Ma (Gauss/Gilbert boundary). From left to right are tuning targets (red - orbital eccentricity; black - orbital insolation at 40°N for the month of June (data from Laskar et al., 2004); stratigraphic classification according to Steenbrink et al. (1999), and Sites Amynteon (KAP-107), Vegora, Lava, and Achlada. For simplicity, only paleomagnetic reversal pattern is shown for each section. For detailed orbital tuning see Fig. 5 and Weber et al. (2010).

9. Photospectrometry as stratigraphic and paleoclimate tool

Initial attempts to identify rhythmic bedding and its relation to orbital forcing concentrated on counting individual beds manually and measuring their thicknesses (e. g., Hilgen et al., 1995). With the implementation of high-resolution rapid scanning techniques, photospectrometry has become very important (e. g., Weber, 1998). It provides a precise digital fingerprint of various geochemical and mineralogical properties that are related to climate and orbital variability. The data yield objective measurements and can be treated mathematically to analyze cyclic behavior and amplitudes of the climatic response. The use of color as high-resolution stratigraphic and paleoenvironmental tool has become increasingly important in recent years (e. g., Debret et al., in press).

The foundation for the KAP-107 tuning is sediment lightness (L^*) or greyscale. Variations mimic rhythmic alternations of relatively bright marls and relatively dark clays or lignites. These changes indicate changes in humidity on precessional time scales. The Ptolemais

Basin is a continental setting in low- to mid-latitudes. Hence, changes in orbital insolation as the ultimate driver of humidity changes have a strong precessional component. Sediments were deposited in shallow water (Kaouras, 1989; van de Weerd, 1983) of an intramontane lacustrine basin. According to the pollen studies of Kloosterboer-van Hove et al. (2006) dark-colored marls of the Ptolemais Basin, which are mostly enriched in clay and/or organic carbon, correspond to relatively dry periods, whereas light-colored marls represent more humid periods.

Changes in humidity are expressed by color component L^* because of the facies change from carbonate-rich (more humid) to clay- or lignite-rich (drier). More arid conditions, on the other hand, exhibit increased redness (enhanced oxic conditions), whereas humid phases were likely more reduced. This relation is clearly shown in Fig. 8 (right), with separate populations for carbonate-rich, clay-rich, and lignite-rich sediment.

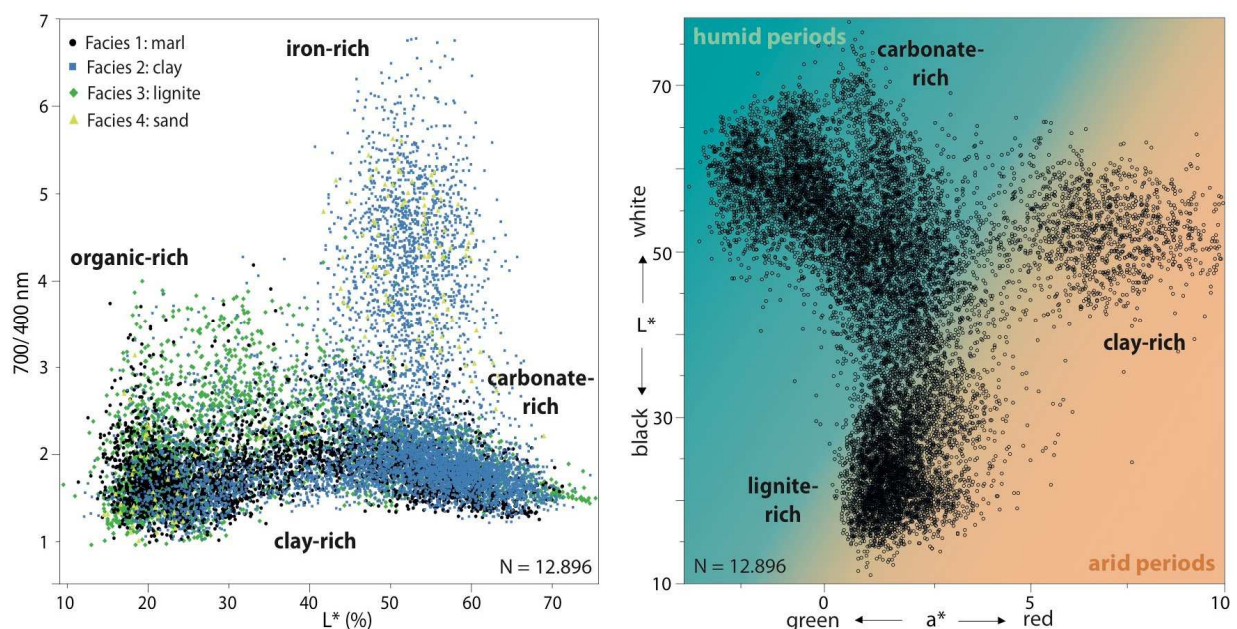


Fig. 8. Sediment color as high-resolution stratigraphic and paleoenvironmental tool. Left shows Q7/4 diagram (Debret et al., in press), i. e., the ratio of reflectance at 700 and 400 nm versus sediment lightness L^* . Note separate populations for carbonate-rich, iron-rich, organic-rich, and clay-rich strata. Right shows L^* versus a^* . Note separate populations for clay-rich, carbonate-rich, and lignite-rich strata.

Debret et al. (in press) introduced the so-called Q7/4 diagram, displaying the ratio of the reflectance between 700 nm and 400 nm versus sediment lightness L^* (Fig. 8, left). Here, lower ratios characterize clays and carbonates, whereas higher ratios indicate sediments rich in organic matter and iron. For the Ptolemais Basin this plot allows to distinguish separate populations for clay-rich, carbonate-rich, and lignite-rich strata with respect to the facies.

10. Summary and conclusions

This study presents a combined approach to establish geological time in sedimentary strata from magnetostratigraphy and orbital tuning. Polarity changes of the Earth's magnetic field provide the basis for the geomagnetic polarity timescale which is well dated for the Late Neogene using radiometric methods. Changes in earth's orbital geometry, on the other

hand, cause changes in insolation, which can also be calculated rather precisely for the Late Neogene. Sedimentary successions are capable of archiving these cyclic changes as rhythmic bedding. We applied this concept of correlating sedimentary cycles to orbital cycles with the aid of magnetic polarity changes to Late Neogene strata from northern Greece.

Lower Pliocene borehole KAP-107 from the Ptolemais Basin shows alternations of marl-rich and clay- or lignite-rich strata. Using ground-truth stratigraphic markers and the magnetic reversal history, we established a low-resolution age model for the borehole spanning 5.1 – 3.1 Ma. Spectral analysis indicates that rhythmic bedding shows two distinct cycles, orbital eccentricity and precession. We used this information to tune the sedimentary record to orbital insolation. As a result, we obtained a high-resolution age model with, ideally, control points at every precession cycle (every 20 kyr). Through correlation of four research sections covering the Ptolemais Basin in a N – S transect, we obtained a complete sedimentary record from the Upper Miocene (7 Ma) to the Upper Pliocene (3 Ma), with the exception of the Messinian Salinity Crisis (5.96 – 5.33 Ma). Conducting the research with high-resolution photospectrometric scanning methods proved very helpful and allows for precise depth age assignments.

11. Acknowledgments

We thank the Public Power Corporation (Ptolemaida) for granting permission to work in their quarries. Also, we wish to thank Greek colleagues Mr. Panagiotis Nikolakakos (Director-general) and Dipl.-Geol. Antonis Nikou (Drilling Section), as well as Daniela Sprenk and Andreas Holzapfel (both University of Cologne) for technical assistance. Supplementary data to this paper are available at doi:10.1594/PANGAEA.770293 (thanks to Hannes Grobe and Rainer Sieger).

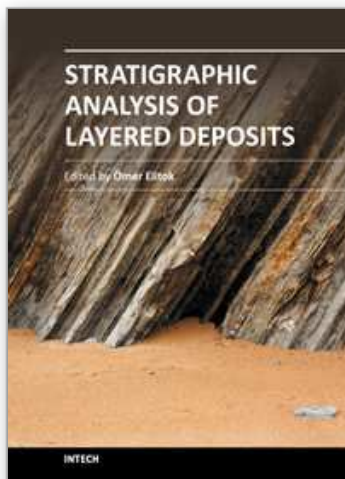
12. References

- Anastopoulos, J. & Koukouzas, C. N. (1972). Economic geology of the southern part of the Ptolemais lignite basin (Macedonia, Greece). *Geol. Geophys. Res.*, Vol. 16, No. 1, pp. 1-189
- Antoniadis, P. A., Blickwede, H. & Kaouras, G. (1994). Petrographical and Palynological analysis on a part (36,0 m – 51,0 m) of a Borehole of the Upper Miocene lignite deposit of Lava-Kozani, N.W. Greece. *Mineral Wealth*, Vol. 91, pp. 7-17
- Berger, A. & Loutre, M. F. (1991). Insolation values for the climate of the last 10 million years. *Quaternary Science Reviews*, Vol. 10, No. 4, pp. 297-317
- Berger, A. L. (1976). Obliquity and precession for the last 5,000,000 years. *Astron. Astrophys.*, Vol. 51, pp. 127-135
- Billups, K. (2002). Late Miocene through early Pliocene deep water circulation and climate change viewed from the sub-Antarctic South Atlantic. *Palaeogeography, Palaeoclimatology, Palaeoecology*, Vol. 185, No. 3-4, pp. 287-307
- Billups, K., Kelly, C. & Pierce, E. (2008). The late Miocene to early Pliocene climate transition in the Southern Ocean. *Palaeogeography, Palaeoclimatology, Palaeoecology*, Vol. 267, No. 1-2, pp. 31-40
- Bornovas, J. & Rondogianni-Tsiambaou, T. (1983). *Geological map of Greece (second edition)*, 1:500.000, Institute of Geology and Mineral Exploration, Athens

- Brierley, C. M., Fedorov, A. V., Liu, Z., Herbert, T. D., Lawrence, K. T. & LaRiviere, J. P. (2009). Greatly Expanded Tropical Warm Pool and Weakened Hadley Circulation in the Early Pliocene. *Science*, Vol. 323, No. 5922, pp. 1714-1718
- Cande, S. C. & Kent, D. V. (1995). Revised calibration of the geomagnetic polarity timescale for the Late Cretaceous and Cenozoic. *Journal of Geophysical Research*, Vol. 100, No. B4, pp. 6093-6095
- CIESM Workshop (2007). The Messinian Salinity Crisis from mega-deposits to microbiology - A consensus report, in: Briand, F. (Ed.), CIESM Workshop Monographs, Monaco, 166 p.
- Debret, M., Sebag, D., Desmet, M., Balsam, W., Copard, Y., Mourier, B., Susperrigui, A. S., Arnaud, F., Bentaleb, I., Chapron, E., Lallier-Vergès, E. & Winiarski, T. (2011). Spectrocolorimetric interpretation of sedimentary dynamics: The new "Q7/4 diagram". *Earth-Science Reviews*, Vol. 109, pp.1-19
- Emeis, K.-C., Sakamoto, T., Wehausen, R. & Brumsack, H.-J. (2000). The sapropel record of the eastern Mediterranean Sea - results of Ocean Drilling Program Leg 160. *Palaeogeography, Palaeoclimatology, Palaeoecology*, Vol. 158, pp. 371-395
- Garcia-Castellanos, D., Estrada, F., Jiménez-Munt, I., Gorini, C., Fernández, M., Vergés, J. & De Vicente, R. (2009). Catastrophic flood of the Mediterranean after the Messinian salinity crisis. *Nature*, Vol. 462, No. 7274, pp. 778-781
- Hays, J. D., Imbrie, J. & Shackleton, N. J. (1976). Variations in the Earth's Orbit: Pacemaker of the Ice Ages. *Science*, Vol. 194, No. 4270, pp. 1121-1132
- Heirtzler, J. R., Dickson, G. O., Herron, E. M., Pitman, W. C., III & Le Pichon, X. (1968). Marine Magnetic Anomalies, Geomagnetic Field Reversals, and Motions of the Ocean Floor and Continents. *J. Geophys. Res.*, Vol. 73, No. 6, pp. 2119-2136
- Hilgen, F. J., Krijgsman, W., Langereis, C. G., Lourens, L. J., Santarelli, A. & Zachariasse, W. J. (1995). Extending the astronomical (polarity) time scale into the Miocene. *Earth and Planet. Sci. Lett.*, Vol. 136, pp. 495-510
- Imbrie, J., Berger, A., Boyle, E. A., Clemens, S. C., Duffy, A., Howard, W. R., Kukla, G., Kutzbach, J., Martinson, D. G., McIntyre, A., Mix, A. C., Molino, B., Morley, J. J., Peterson, L. C., Pisias, N. G., Prell, W. L., Raymo, M. E., Shackleton, N. J. & Toggw. (1993). On the structure and origin of major glaciation cycles. *Paleoceanography*, No. 8(6), pp. 699-735
- Imbrie, J., Hays, J.D., Martinson, D.G., McIntyre, A., Mix, A.C., Morley, J.J., Pisias, N.G., Prell, W.L., Shackleton, N.J. (1984). The orbital theory of Pleistocene climate: Support from a revised chronology of the marine $\delta^{18}\text{O}$ record, in: Berger, A.L., Imbrie, J., Hays, J., Kukla, G., Saltzman, B. (Eds.). D. Reidel, Dordrecht, pp. 269-305
- Kaouras, G. (1989). *Kohlepetrographische, palynologische und sedimentologische Untersuchungen der pliozänen Braunkohle von Kariochori bei Ptolemais/NW-Griechenland*, PhD, 258p., Georg-August-Universität, Göttingen
- Kloosterboer-van Hove, M. L., Steenbrink, J., Visscher, H. & Brinkhuis, H. (2006). Millennial-scale climatic cycles in the Early Pliocene pollen record of Ptolemais, northern Greece. *Palaeogeogr. Palaeoclimatol. Palaeoecol.*, Vol. 229, pp. 321-334
- Koukouzas, N., Kalaitzidis, S. P. & Ward, C. R. (2010). Organic petrographical, mineralogical and geochemical features of the Achlada and Mavropigi lignite deposits, NW Macedonia, Greece. *International Journal of Coal Geology*, Vol. 83, No. 4, pp. 387-395
- Koukouzas, N., Ward, C. R., Papanikolaou, D. & Li, Z. (2009). Quantitative Evaluation of Minerals in Lignites and Intraseam Sediments from the Achlada Basin, Northern Greece. *Energy & Fuels*, Vol. 23, No. 4, pp. 2169-2175

- Krijgsman, W., Hilgen, F. J., Langereis, C. G., Santarelli, A. & Zachariasse, W. J. (1995). Late Miocene magnetostratigraphy, biostratigraphy and cyclostratigraphy in the Mediterranean. *Earth Planet. Sci. Lett.*, Vol. 136, pp. 475-494
- Krijgsman, W. F., Hilgen, J., Raffi, I., Sierro, J. & Wilson, D. S. (1999). Chronology, causes and progression of the Messinian salinity crisis. *Nature*, Vol. 400, pp. 625-655
- Kuiper, K. F. (2003). *Direct intercalibration of radio-isotopic and astronomical time in the Mediterranean Neogene*, PhD, 223p., Utrecht University, Utrecht
- Kuiper, K. F., Hilgen, F. J., Steenbrink, J. & Wijbrans, J. R. (2004). $^{40}\text{Ar}/^{39}\text{Ar}$ ages of tephrae intercalated in astronomically tuned Neogene sedimentary sequences in the eastern Mediterranean. *Earth and Planetary Science Letters*, Vol. 222, No. 2, pp. 583-597
- Langereis, C. G. & Hilgen, F. J. (1991). The Rossello composite: a Mediterranean and global reference section for the Early to early Late Pliocene. *Earth Planet. Sci. Lett.*, Vol. 104, pp. 211-225
- Laskar, J., Robutel, P., Joutel, F., Gastineau, M., Correia, A. C. M. & Levrard, B. (2004). A long-term numerical solution for the insolation quantities of the Earth. *Astronomy and Astrophysics*, Vol. 428, pp. 261-285
- Lomb, N. R. (1976). Least-squares frequency analysis of unequally spaced data. *Astrophysics and Space Science*, Vol. 39, pp. 447-462
- Milankovitch, M. (1941). *Kanon der Erdbestrahlung und seine Anwendung auf das Eiszeitenproblem* (edition), Belgrad
- Mudelsee, M. & Raymo, M. E. (2005). Slow dynamics of the Northern Hemisphere glaciation. *Paleoceanography*, Vol. 20, pp. 1-14
- Paillard, D. (1996). Macintosh Program Performs Time-Series Analysis, EOS.
- Pavlidis, S. B. & Mountrakis, D. M. (1987). Extensional tectonics of northwestern Macedonia, Greece, since the late Miocene. *J. Struct. Geol.*, Vol. 9, No. 4, pp. 385-392
- Ravelo, A. C., Andreasen, D. H., Lyle, M., Lyle, A. O. & Wara, M. W. (2004). Regional climate shifts caused by gradual global cooling in the Pliocene epoch. *Nature*, Vol. 429, pp. 263-267
- Ravelo, A. C., Dekens, P. S. & McCarthy, M. (2006). Evidence for El Niño-like conditions during the Pliocene. *GSA Today*, Vol. 16, No. 3, pp. 4-11
- Ruddiman, W. (2004). The Role of Greenhouse Gases in Orbital-Scale Climatic Changes. *Eos*, Vol. 85, No. 1, pp. 6-7
- Ruggieri, E., Herbert, T., Lawrence, K. T. & Lawrence, C. E. (2009). Change point method for detecting regime shifts in paleoclimatic time series: Application to $\delta^{18}\text{O}$ time series of the Plio-Pleistocene. *Paleoceanography*, Vol. 24, No. 1, pp. 1-15
- Scargle, J. D. (1982). Studies in astronomical time series analysis. II. Statistical aspects of spectral analysis of unevenly spaced data. *The Astrophysical Journal*, Vol. 263, pp. 835-853
- Scargle, J. D. (1989). Studies in astronomical time series analysis. III. Fourier transforms, autocorrelation functions, and cross-correlation functions of unevenly spaced data. *The Astrophysical Journal*, Vol. 343, No. 133, pp. 874-887
- Schulz, M. & Mudelsee, M. (2002). REDFIT: estimation red-noise spectra directly from unevenly spaced paleoclimatic time series. *Computer & Geosciences*, Vol. 28, pp. 421-426
- Shackleton, N. J., Backmann, J., Zimmermann, H., Kent, D. V., Hall, M. A., Roberts, D. G., Schnitker, D., Baldauf, J. G., Desprairies, H., R., Huddleston, P., Keene, J. B.,

- Kaltenback, A. J., Krumsiek, K. A. O., Morton, A. C., Murray, J. W. & al, e. (1984). Oxygen isotope calibration of the onset of ice-rafted and history of glaciation in the North Atlantic region. *Nature*, No. 307, pp. 620-623
- Steenbrink, J. (2001). *Orbital signatures in lacustrine sediments*, PhD Thesis, 167p., Utrecht University, Utrecht
- Steenbrink, J., Hilgen, F. J., Krijgsman, W., Wijbrans, J. R. & Meulenkamp, J. E. (2006). Late Miocene to Early Pliocene depositional history of the intramontane Florina-Ptolemais-Servia Basin, NW Greece: Interplay between orbital forcing and tectonics. *Palaeoecology*, Vol. 238, pp. 151-178
- Steenbrink, J., van Vugt, N., Hilgen, F. J., Wijbrans, J. R. & Meulenkamp, J. E. (1999). Sedimentary cycles and volcanic ash beds in the Lower Pliocene lacustrine succession of Ptolemais (NW Greece): discrepancy between $^{40}\text{Ar}/^{39}\text{Ar}$ and astronomical ages. *Palaeogeography, Palaeoclimatology, Palaeoecology*, Vol. 152, pp. 283-303
- Steenbrink, J., van Vugt, N., Kloosterboer-van Hoeve, M. L. & Hilgen, F. J. (2000). Refinement of the Messinian APTS from sedimentary cycle patterns in the lacustrine Lava section (Servia Basin, NW-Greece). *Earth and Planetary Science Letters*, Vol. 181, pp. 161-173
- Tougiannidis, N. (2009). *Karbonat- und Lignitzyklen im Ptolemais-Becken: Orbitale Steuerung und suborbitale Variabilität (Spätneogen, NW Griechenland). Sedimentologische Fallstudie unter Berücksichtigung gesteinsmagnetischer Eigenschaften*, PhD Thesis, 122p., Institute of Geology and Mineralogy, University of Cologne, Cologne
- van de Weerd, A. (1983). Palynology of some upper Miocene and Pliocene Formations in Greece. *Geologisches Jahrbuch*, Vol. 48, pp. 3-63
- van Vugt, N., Langereis, C. G. & Hilgen, F. J. (2001). Orbital forcing in Pliocene - Pleistocene Mediterranean lacustrine deposits: dominant expression of eccentricity versus precession. *Paleogeography, Paleoclimatology, Paleoecology*, Vol. 172, pp. 193-205
- van Vugt, N., Steenbrink, J., Langereis, C. G., Hilgen, F. J. & Meulenkamp, J. E. (1998). Magnetostratigraphy-based astronomical tuning of the early Pliocene lacustrine sediments of Ptolemais (NW Greece) and bed-to-bed correlation with the marine record. *Earth and Planetary Science Letters*, Vol. 164, pp. 535-551
- Weber, M. E. (1998). Estimation of biogenic carbonate and opal by continuous non-destructive measurements in deep-sea sediments: application to the eastern Equatorial Pacific. *Deep-Sea Research 1*, Vol. 45, pp. 1955-1975
- Weber, M. E., Mayer, L. A., Hillaire-Marcel, C., Bilodeau, G., Rack, F., Hiscott, R. N. & Aksu, A. E. (2001). Derivation of $\delta^{18}\text{O}$ from sediment core log data: Implications for millennial-scale climate change in the Labrador Sea. *Paleoceanography*, Vol. 16, No. 0, pp. 1-12
- Weber, M. E., Tougiannidis, N., Kleineder, M., Bertram, N., Ricken, W., Rolf, C., Reinsch, T. & Antoniadis, P. (2010). Lacustrine sediments document millennial-scale climate variability in northern Greece prior to the onset of the northern hemisphere glaciation. *Palaeogeography, Palaeoclimatology, Palaeoecology*, Vol. 291, No. 3-4, pp. 360-370
- Zijderveld, J.D.A. (1967). A.C. demagnetization of rocks: analysis of results, in: Collinson, D.W.e.a. (Ed.), *Methods in Palaeomagnetism*. Elsevier, Amsterdam, pp. 254-286



Stratigraphic Analysis of Layered Deposits

Edited by Dr. Ömer Elitok

ISBN 978-953-51-0578-7

Hard cover, 298 pages

Publisher InTech

Published online 27, April, 2012

Published in print edition April, 2012

Stratigraphy, a branch of geology, is the science of describing the vertical and lateral relationships of different rock formations formed through time to understand the earth history. These relationships may be based on lithologic properties (named lithostratigraphy), fossil content (labeled biostratigraphy), magnetic properties (called magnetostratigraphy), chemical features (named chemostratigraphy), reflection seismology (named seismic stratigraphy), age relations (called chronostratigraphy). Also, it refers to archaeological deposits called archaeological stratigraphy. Stratigraphy is built on the concept "the present is the key to the past" which was first outlined by James Hutton in the late 1700s and developed by Charles Lyell in the early 1800s. This book focuses particularly on application of geophysical methods in stratigraphic investigations and stratigraphic analysis of layered basin deposits from different geologic settings and present continental areas extending from Mexico region (north America) through Alpine belt including Italy, Greece, Iraq to Russia (northern Asia).

How to reference

In order to correctly reference this scholarly work, feel free to copy and paste the following:

M.E. Weber, N. Tougiannidis, W. Ricken, C. Rolf, I. Oikonomopoulos and P. Antoniadis (2012). Orbital Control on Carbonate-Lignite Cycles in the Ptolemais Basin, Northern Greece - An Integrated Stratigraphic Approach, Stratigraphic Analysis of Layered Deposits, Dr. Ömer Elitok (Ed.), ISBN: 978-953-51-0578-7, InTech, Available from: <http://www.intechopen.com/books/stratigraphic-analysis-of-layered-deposits/orbital-control-on-carbonate-lignite-cycles-in-the-ptolemais-basin-northern-greece-an-integrate>

INTECH
open science | open minds

InTech Europe

University Campus STeP Ri
Slavka Krautzeka 83/A
51000 Rijeka, Croatia
Phone: +385 (51) 770 447
Fax: +385 (51) 686 166
www.intechopen.com

InTech China

Unit 405, Office Block, Hotel Equatorial Shanghai
No.65, Yan An Road (West), Shanghai, 200040, China
中国上海市延安西路65号上海国际贵都大饭店办公楼405单元
Phone: +86-21-62489820
Fax: +86-21-62489821

© 2012 The Author(s). Licensee IntechOpen. This is an open access article distributed under the terms of the [Creative Commons Attribution 3.0 License](#), which permits unrestricted use, distribution, and reproduction in any medium, provided the original work is properly cited.

IntechOpen

IntechOpen